Luminescence and vibronic structure in $Ca_{1-x}Sr_xF_2:Eu^{2+}$ mixed crystals

1991 J. Phys.: Condens. Matter 3 5903

(http://iopscience.iop.org/0953-8984/3/31/013)

J. Phys.: Condens. Matter 3 (1991) 5903–5913. Printed in the UK

Luminescence and vibronic structure in $Ca_{1-x}Sr_xF_2:Eu^{2+}$ mixed crystals

R Nakata, H Satoh, J Tominaga, K Kawano and M Sumita
Department of Electronics Engineering, The University of Electro-Communications, Chofu-shi, Tokyo 182, Japan

Received 7 January 1991, in final form 25 March 1991

Abstract. The optical properties and vibronic structures in the luminescence were studied for $Ca_{1-x}Sr_xF_2$ mixed crystals doped with Eu^{2+} ions. The peak energy, linewidth, lifetime and non-radiative activation energy showed a non-linear variation with increasing x. The x-dependence of the zero-phonon line position and its linewidth revealed electron–phonon coupling in the weak range (Huang–Rhys factor $S < 3$). This originates from local lattice distortion of the mixed crystal. The calculated results of vibronic structures successfully explained the spectral lineshape of the sideband by superposing the excited state phonon modes onto their ground-state multiple-phonon modes.

1. Introduction

The incorporation of an impurity in a lattice exhibits a unique point of symmetry, in which the lattice is locally perturbed by the differences in the effective mass and force constant on a centralized impurity ion. The deviation from inversion symmetry at the ionic site influences the intensity and the lineshape of the optical spectrum. The parity-forbidden transitions are often broken. Then, as a dynamic aspect of crystal distortion, the phonon plays a major role (Bartolo 1968, Fitchen 1968, McClure 1966, Rebane 1970). There is, however, a specific feature for rare-earth ions in solids, i.e. the 4f–electron shell is almost totally shielded inside the ions. So the effects of external distortion are relatively weak in contrast with the 3d transition-metal ions which exhibit strong interactions with the lattices. As the doped ion of the ground state with no orbital degeneracies is inherent in a high crystal symmetry, the electric dipole transition is strongly forbidden. One condition to relax this restriction is the preparation of mixed crystals in which the crystal symmetry is lowered. Another is configuration mixing which induces a great variation in the oscillator strength between the impurity–host combinations. Optical transitions through f–d configuration mixing generally manifest a vibronically broadened band. These features may lead us to suggest that scintillators with long-wavelength sensitivity as well as phonon-terminated tunable lasers are possible (Ehrlich 1978, 1980, McCumber 1964, Walling 1987).

Hobden (1965) first observed the vibronic structures of $CaF_2:Eu^{2+}$ to originate from the first excited state of the $4f^65d$ configuration. He partially determined their phonon structures by comparison with the results for Sm^{2+}, Tm^{2+} and H^- in CaF_2. Using optical detection of paramagnetic resonance, Chase (1970) found the Γ_8 lowest quartet of the

0953-8984/91/315903 + 11 $03.50

$4f^6 5d$ configuration in CaF_2:Eu and SrF_2:Eu to exhibit the dynamic Jahn–Teller effect and estimated the excited vibronic components as within 10 cm^{-1}. For the CaF_2–SrF_2 mixed system, however, no estimates of the electron–phonon coupling strength have been carried out and no spectral properties of the zero-phonon line have been determined in a systematic manner. Recently, Kawano *et al* (1990) reported that in $Ca_{1-x}Sr_xF_2$ mixed crystals the luminescence peak energy shifted to lower energies than in CaF_2 or SrF_2. Simultaneously, the linewidth broadened considerably and the activation energy of the non-radiative recombination lessened. We proposed that these anomalous behaviours were explained by enhancing the electron–phonon coupling, indicating the calculation results of the half-width and the quantum efficiency. In this work, we present a radiative-to non-radiative transition process from the results of lifetimes and spectral intensities of the luminescence in the mixed system $Ca_{1-x}Sr_xF_2$:Eu and clarify the phonon structures which contribute most to electron–phonon coupling from analyses of the vibronic structures obtained.

2. Experimental methods

The mixed system of CaF_2 and SrF_2 with a molar composition was prepared with a fixed doping content of $EuCl_3 \cdot 6H_2O$ from 0.01 to 2.0 mol%. All measurement results obtained are for crystals doped with 0.05 mol% except for the concentration dependence results. Crystal growth was performed with a Bridgman induction furnace up to a maximum power of 15 kW under 300 kHz oscillation (this furnace was manufactured by Dai-ichi Dentsu Co., Chofu, Tokyo). The crystal crucible, supplied by Tohkai Carbon Co., Nagoya, was made of high-purity carbon in which contamination was no higher than 25 ppm. The crucible had a cylindrical shape of diameter 60 mm and 100 mm long. Seven end-tapered holes of diameter 9 mm and 30 mm depth were distributed at regular intervals on the upper surface of the cylindrical axis. Thus seven crystals with different mixed compositions were grown simultaneously under the same conditions to hold constant the composition ratios after growth. However, no check of the crystals grown was carried out by any method.

The measurements of absorption, excitation and luminescence spectra were made using a spectrophotometer and fluorophotometer. At low temperatures, a set-up with a helium glass Dewar, a monochromator and a superhigh-pressure Hg or Xe lamp was used; the details have been described previously (Kawano *et al* 1990). The optical spectra were also examined with a spectrometric multichannel analyser system (Princeton Instruments IRY-1024 USA), known as the SMA, with a monochromator (Jobin–Yvon HR-320). To measure the lifetimes, a YAG laser system (JK laser model DLPY4, UK) was used with a pulse duration of 25 ns under Q-switch operation. The high-speed pulse was memorized using a storagescope triggered by a strobe signal from the YAG laser. The two-photon response experiment was carried out in the tuning range 685–704 nm with a linewidth of 0.1 cm^{-1}, using a laser dye LD700 (Exciton Inc. USA) solution pumped by a second-harmonic wave ($\lambda = 532$ nm) of the YAG laser.

3. Experimental results

3.1. Absorption, excitation and luminescence

The absorption spectra are composed of two main broad bands whose peaks are 214.3 nm and 334.0 nm at room temperature. These bands are assigned (Chase 1970) to $4f^6\ {}^7F_J$-coupled t_{2g} and e_g bands, respectively, with a splitting factor $Dq \simeq 1670$ cm^{-1} in the $4f^6 5d$

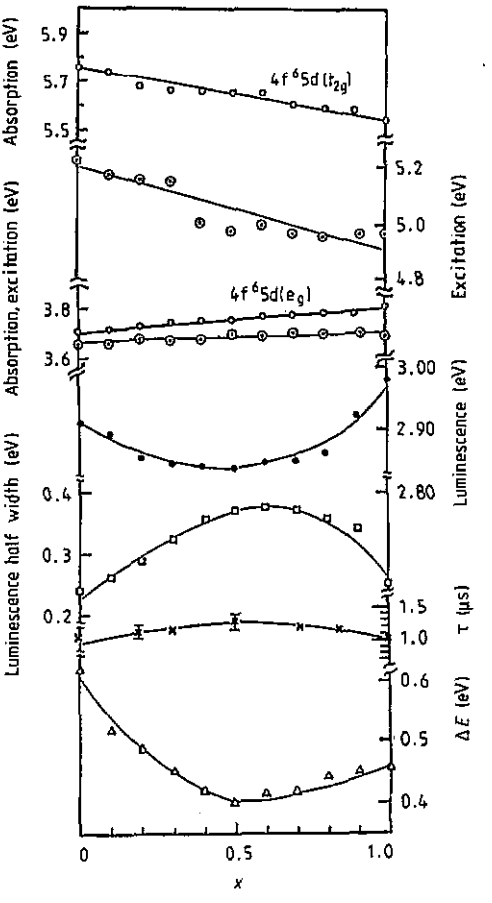

Figure 1. Variations in the absorption (○), excitation (⊙) and luminescence (●) peaks, the half-width (□), the lifetime τ (×) and the non-radiative activation energy ΔE (△) as functions of x in mixed $Ca_{1-x}Sr_xF_2:Eu^{2+}$ crystals.

configuration when the ground state is $^8S_{5/2}$ in $4f^7$. The traces of exchange-coupled $4f^6$ electrons appear as seven fine structures from $^7F_0$ to $^7F_6$ on the lower-energy side of the e_g band, which is shown together with the vibronic sideband, as mentioned in section 3.3. The luminescence band appears at 424.6 nm by exciting either of the two absorption bands. By monitoring the luminescence peak band, we observed two excitation bands at 236.5 and 335.0 nm, in which the intensity of the former was one third that of the latter.

There are several points characteristic to the luminescence, which correlate with the previous work (Kawano *et al* 1990). With increasing x in $Ca_{1-x}Sr_xF_2:Eu$ mixed crystals, the absorption and excitation peaks vary linearly from CaF_2 to SrF_2, while the luminescence moved parabolically so as to reach an extremum around $x = 0.5$. These behaviours are precisely shown in figure 1, including the variation in the lifetime τ. The temperature dependences of the luminescence intensity and its lifetime revealed a minimum down to 0.4 eV in the activation energy to non-radiative relaxation. These thermal activation processes for each x have agreed well with the Arrhenius-type plots of quantum efficiencies. In addition, the lifetime τ showed a slightly increasing tendency around $x = 0.5$ even when experimental errors were considered. In the measurements of the luminescence wavelength, we took care that the wavelength of the exciting light

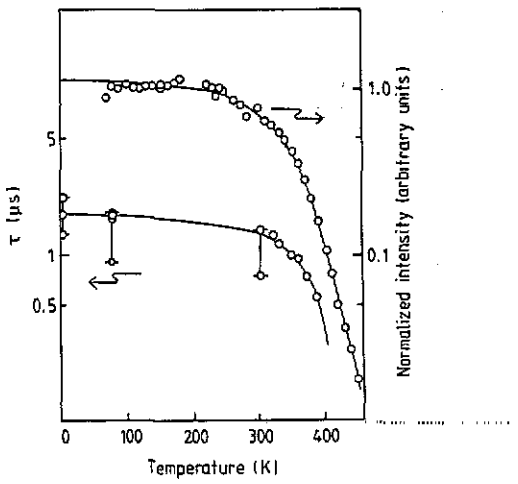

Figure 2. Temperature dependences of the normalized intensity and the lifetime τ for the luminescence of $CaF_2:Eu^{2+}$.

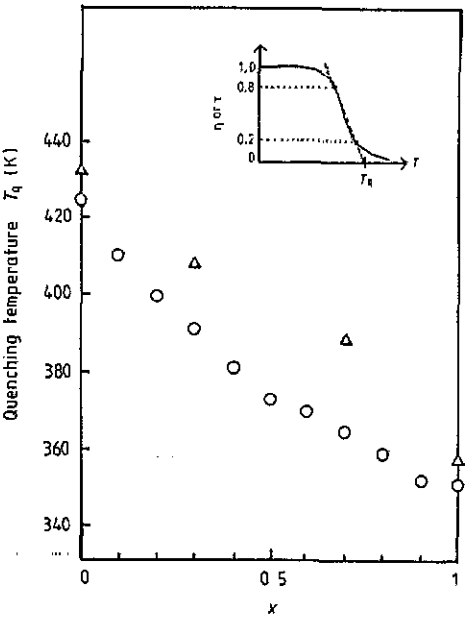

Figure 3. The x-dependence of the quenching temperature T_q obtained by measuring the luminescence intensity η (○) and the lifetime τ (△) for $Ca_{1-x}Sr_xF_2:Eu^{2+}$. T_q is defined for T-dependences of τ and η, as shown in the inset.

was adjusted to that of the absorption peak because the latter had varied with x. By using the best fit with experimental points, the peak energy E_a of the e_g absorption band as a function of x is written in electronvolts as follows:

$$E_a = 3.712 + 0.068x. \tag{1}$$

On the other hand, the luminescence peak energy E_l is given by

$$E_l = 0.434x^2 - 0.371x + 2.917. \tag{2}$$

By subtracting equation (2) from equation (1), we find that the Stokes energy has a maximum of 1.017 eV at $x = 0.506$ whereas, for $x \approx 0$ and 1.0, it has a maximum at 0.8 eV.

3.2. Luminescence intensity, lifetime and two-photon response

The luminescence intensity and the lifetime were measured in the temperature range from 4.2 to 450 K. The typical results for $CaF_2:Eu$ are shown in figure 2. The quantum efficiency decreases slowly with rising temperature until about 240 K, and decays exponentially. The lifetime also holds for 1–2 μs up to RT and subsequently decreases abruptly. This is understood (Kawano *et al* 1990) in terms of thermal activation decay that the purely radiative emission is competing with non-radiative and with phonon-assisted (vibronic) processes which are responsible for the thermal shortening of the lifetime. Above 450 K, no luminescence of any crystals was detectable within the sensitivities of the instruments, in which a quenching temperature T_q is defined in figure 3.

The x-dependence of T_q monotonically decreases from CaF_2 (T_q = 425 K) to SrF_2 (T_q = 350 K), as shown in this figure. This evidence contrasts with the non-linear behaviours of peak position, half-width and lifetime.

The lifetime measurement using two photon absorption was carried out by monitoring the luminescence band from 190 K to RT. Then the absorption corresponds to a transition from ^8S to excited ^6P levels in the $4f^7$ configuration which is inaccessible by single-photon spectroscopy. The temperature dependence of the lifetime for two-photon absorption showed a very similar result to that in the case of a single photon, which was 1–2 μs in the measured temperature range. Moreover, no symptoms of multidecay processes were observed. This result confirmed that the final emitted level was restricted to the lowest Γ_8 level of the e_g band as well as the occurrence of a very efficient non-radiative relaxation. Downer *et al* (1983) carried out two-photon spectroscopy on the excited $^6P_{7/2}$ and $^6P_{5/2}$ levels and concluded that the luminescence from the Γ_8 level eventually played the role of a terminated level in this emission process.

The peak energy, half-width and normalized intensity in the luminescence band did not vary in the Eu^{2+} concentration range from 0.02 to 0.2 mol%. Heavily doped crystals above 0.2 mol% lead to light quenching as the result of reabsorption of emission with a red shift in the peak energy, while the half-width shows a slow decrease. This concentration dependence confirms that the energy transfer process between the paramagnetic impurities has a lower possibility than the thermal transfer process.

3.3. Vibronic structures

With decreasing temperature, the half-linewidth of the luminescence band narrowed gradually, and the temperature dependence agreed well with the calculation result based on the theory of electron–phonon interactions, as mentioned in the previous paper (Kawano *et al* 1990). For CaF_2:Eu at 4.2 K, we observed an intense zero-phonon line at 24 177.0 cm^{-1} and the vibronic structures superposed on the broad sideband of width 900 cm^{-1}. From the assignments of the periodical phonon frequency in the vibronic structures, the observed phonon frequencies consist of three fundamental frequencies at 177.1, 267.0 and 391.5 cm^{-1}, plus their multiple and combined frequencies. On the other hand, the vibronic structures in the absorption band are at 126.0, 283.5 and 346.5 cm^{-1}. The agreement between these values and those obtained by Hobden (1965) is not very good, starting with his zero-phonon frequency 24 206 cm^{-1}. This is possibly owing to the slightly inferior resolution of our monochromator as well as to the much higher Eu^{2+} concentration in our specimens. In the case of SrF_2:Eu, the zero-phonon frequency of 24 937.5 cm^{-1} and its vibronic structures appeared in an analogous manner to those of CaF_2:Eu. The vibronic spectra of the e_g absorption and the luminescence for CaF_2:Eu and SrF_2:Eu are shown in figures 4(*a*) and 4(*b*), respectively. From precise comparisons between the vibronic structures of absorption and luminescence, we see that the vibration energy $\hbar\omega_e$ in the excited state is 10–30% larger than the vibration energy $\hbar\omega_g$ in the ground state. The curvature ratio of the adiabatic potential of the e_g excited state becomes less than that of the ground state because of the effect of the second-order perturbation. We also find in this figure that no mirror image between absorption and luminescence is observed. Such a lack of symmetry comes from the effect of the second-order perturbation in the adiabatic potential (Fitchen 1968) as well as the Jahn–Teller distortion proposed by Chase (1970) from the magneto-optical experiment on the excited e_g band.

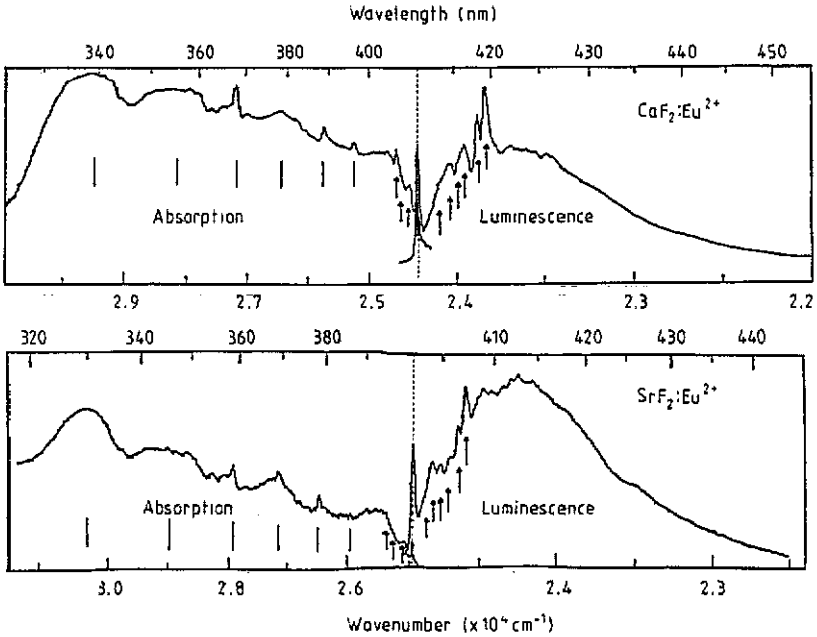

Figure 4. The vibronic structures for the absorption (only the e_g band) and the luminescence of $CaF_2:Eu^{2+}$ and $SrF_2:Eu^{2+}$ using unpolarized light at 4.2 K: ·····, zero-phonon line for which the scale of the abscissa is different on each side of this line; ↑, observed phonon structures; |, predicted line positions of $^7F_6$ to $^7F_0$ in the free states of the $4f^6$ configuration. The upper axes on each part give the wavelength (nm) and the lower axes give the wavenumber ($\times 10^4$ cm^{-1}).

The e_g absorption band has seven fine-structure lines superposed on its low-energy side. They are 4500 cm^{-1} wide, and the separation between the structures narrows towards the lower energies. In view of the similar structures observed for the Eu^{2+} ion in some host crystals (Ryan *et al* 1974), the structures are ascribed to ^7F_J structures (from $^7F_0$ to $^7F_6$) because of the $4f^6$ core configuration perturbed by octahedral ligands. Using the spin–orbit parameter λ of 250 cm^{-1} proposed by Weakliem (1972), we predicted their positions in the free states as shown in figure 4; the agreement is good. A markedly broad half-width of 2500 cm^{-1} for absorption compared with 1000 cm^{-1} for luminescence is dominantly due to this $4f^6$ core band, and so the sideband width for absorption is actually only 800 cm^{-1}.

The temperature dependence of the vibronic structure was measured from 4.2 to 100 K. With rising temperature, the intensities of both the zero-phonon line and the phonon sideband decrease while their positions shift to lower energies. In the temperature range above 120 K, they are smeared out in the luminescence band. As a typical example of $CaF_2:Eu$, the intensity ratio of the total vibronic structure to the zero-phonon line was plotted as a function of temperature, together with the variations in the half-width and the shift of the zero-phonon line, as shown in figure 5. From the analysis of vibronic structures with respect to ω_g for the luminescence, we can regard the effect of second-order perturbation as negligibly small, since the energy separation between the ground ^8S and the excited e_g states is larger than 3×10^4 cm^{-1}. Therefore, on the

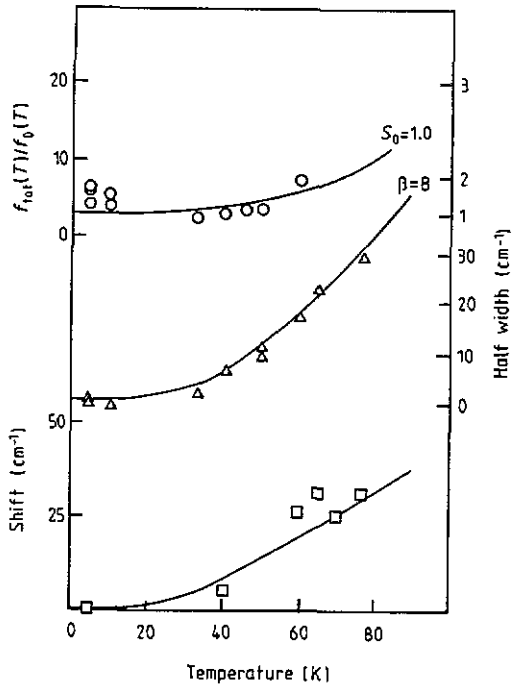

Figure 5. Temperature dependences of the intensity ratio (○) of the total vibronic structure to the zero-phonon line, of the half-width (△) and of the shift in energy (□) of the zero-phonon line for CaF_2: Eu^{2+}: ——, calculated with the determined parameters using equations (3)–(6) in the text.

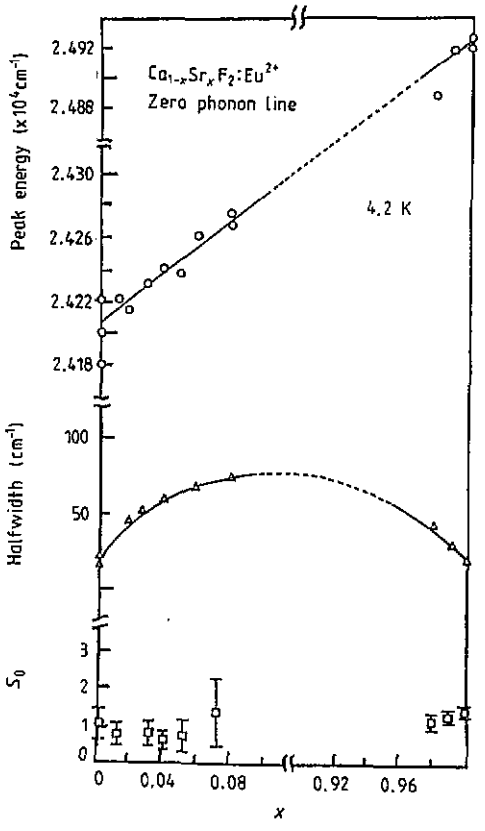

Figure 6. Variations in the peak energy (○), the half-width (△) of the zero-phonon line and the S_0-value (□) with x, in which sharp vibronic structures are observed only in the vicinity of $x = 0$ and 1.0.

assumption of a linear electron–phonon coupling on the basis of the configuration coordinate model (Fitchen 1968, McClure 1966, Rebane 1970), the Huang–Rhys factor $S(T)$ is given by

$$S(T) = S_0 \coth(\hbar\omega_a/2kT) \tag{3}$$

where S_0 is the S-value at 0 K and ω_a is the average phonon frequency. The frequency shift of the zero-phonon line from the position at 0 K is derived as

$$\Delta\Omega = \alpha[\coth(\hbar\omega_a/2kT) - 1]. \tag{4}$$

The half-linewidth W_d of the zero-phonon line is related to the second moment $M_2 = S\hbar^2\omega_a^2 \coth(\hbar\omega_a/2kT)$ of the band shape and is given by

$$W_d = \sqrt{\beta[\coth^2(\hbar\omega_a/2kT) - 1]}. \tag{5}$$

When the transition probabilities for the zero-phonon and one-phonon cases are set at $W^{(0)}$ and $W^{(1)}$, respectively, where $W^{(0)} \gg W^{(1)}$, then the intensity of the zero-phonon

line is approximated by $f_0(T) = W^{(0)} \exp[-S(T)]$ and the intensity of the total vibronic lines for $f_{tot}(T) = W^{(1)} \coth(\hbar\omega_a/kT)$. Accordingly, the following relation is also derived:

$$f_0(T)/f_{tot}(T) = \exp[-S(T)]. \tag{6}$$

Following the above equations (3)–(6), the calculated lines are drawn with a best fit for the parameters $\alpha = 25$, $\beta = 8$ and $S_0 = 1.0$ at $\omega_a = 4.6 \times 10^{13}\ s^{-1}$, as shown in figure 5. The agreement with experimental points is so good that the linear coupling approximation is regarded as valid. Also the magnitudes of the determined parameters are comparable with those of weak electron–phonon systems such as Eu^{2+}- and Sm^{2+}-doped alkali halides (Baldini and Guzzi 1968). With increasing x, the intensities of the vibronic structures with a zero-phonon line gradually decrease and they become buried in the intense luminescence band for $x > 0.2$. As x approaches 1.0, however, they are again restored and the spectrum approaches that for SrF_2: Eu. From equation (6), the decrease in the intensity of the zero-phonon line may suggest an increase in the S-factor. For crystals with a large x, some weak harmonics are sometimes observed because, the greater the number of vibration species, the more combined phonon modes must be considered. However, they were not clearly identified as they were masked by the luminescence band. The position of the zero-phonon line and the S_0-value estimated from equations (3) and (6) against x are shown in figure 6. The linear variation in the zero-phonon line position against the x-value implies that the electronic transition irrelevant to excited phonons changes monotonically with the variation in the lattice parameter from CaF_2 to SrF_2. On the other hand, the S_0-value does not have a clear dependence on the x-value, showing dissipation in the small range of $S = 1$–2. The absolute magnitude of the S_0-value is too small to determine the degree of phonon coupling directly.

A clear zero-phonon line appears on subtraction of the background of the phonon sideband from the total vibronic structure. This directly reflects the degree of lattice mismatch and strain in the crystal because of its pure electronic transition without the assistance of phonons. The lineshape of the zero-phonon line depends on the composition of the mixed crystal as well as the concentration of impurities. With increasing x, the shape gradually changes from Lorentzian to Gaussian, resulting in an increase in the half-width, as shown in figure 6. This suggests that the mixed-crystal effect creates the zero-phonon line as an inhomogeneous line which consists of many homogeneous emission lines corresponding to the number of impurity ions in different environmental sites.

4. Discussion

On variation in x, the peak energy, linewidth and non-radiative activation energy in the luminescence band showed non-linear parabolic behaviours including the new fact that the lifetime was slightly prolonged at around $x = 0.5$. This has been explained by enlarging the electron–phonon coupling on the basis of the configuration coordinate scheme (Kawano *et al* 1990). The mixed CaF_2–SrF_2 crystals provide a configuration of ligands based on the weight average around a Eu^{2+} ion according to its mixed composition. As the crystal field is different for each Eu^{2+} ion, the luminescence energy may be dispersed so inhomogeneously as to end up by increasing the half-width. We propose, however, that the possibility of inhomogeneous broadening is actually small if we consider universal non-linearities in the peak energy as well as in ΔE against the precise

variation in x. The inhomogeneous effect appears in the changes in the lineshape and the half-width of the zero-phonon line. In the present work, analyses of vibronic structure give further support for the interpretation of the previous work.

The predicted phonons for fluorite crystals with the space group O_h^5 are composed of nine kinds of host mode in which LO_1, TO_1 and $LO_2(\equiv TO_2)$ modes are excited at the Γ point (Bartolo 1968). Comparing the observed vibronic frequencies with the results obtained from infrared (Ryan *et al* 1974), dispersion (Kaiser *et al* 1962) and neutron (Gribier *et al* 1962) experiments, we can ascribe ν_1 (177.1 cm^{-1}), ν_2 (267.0 cm^{-1}) and ν_3 (391.5 cm^{-1}) to one localized T_{1u} mode, and two host modes TO_1 and LO_1, respectively. In these assignments of lattice modes, the deviation in frequencies by the square root $\sqrt{M_{Ca}/M_{Eu}}$ of the mass ratio, is considered to take into account substitutional impurities. The transition probability for one phonon with frequency ω is as follows:

$$W^{(1)}(\omega) = \sum_{k=1}^{N} S_k \exp(-S)\,\delta(\omega - \omega_k). \tag{7}$$

The n-phonon probability as an n-fold convolution scheme of one phonon, i.e.

$$W^{(n)}(\omega) = \frac{1}{n!}\int_0^{\omega_{max}} W^{(1)}(\omega_1)\,d\omega_1 \int_0^{\omega_{max}} W^{(1)}(\omega_2)\delta(\omega - \omega_1 - \omega_2)\,d\omega_2$$
$$\ldots \int_0^{\omega_{max}} W^{(1)}(\omega_n)\delta(\omega - \omega_1 - \omega_2 \ldots - \omega_n)\,d\omega_n \tag{8}$$

is derived assuming the frequencies of coupled modes extended to ω_{max}. From the relation $E_1 = E_0 - n\hbar\omega$ between the luminescence energy $E_1(=h\nu)$ and the zero-phonon energy E_0, the lineshape function is given as follows:

$$\int_0^{\infty} W(\nu)\,d\nu = \frac{S^n}{n!}\exp(-S) \tag{9}$$

where $\Sigma_{n=0}^{\infty} W^{(n)}(\nu) = W(\nu)$ and $\int_0^{\infty} W(\nu)\,d\nu = 1$ are assumed. This relation indicates that a lineshape function is approximated as that of the Poisson distribution for the one-phonon mode with its S-value. Then the total S-value of the N excited modes is given as a summation of S_k in each phonon k-mode. So the coupling strength by definite modes at CaF_2 or SrF_2 is distributed by many weakly coupled modes in the mixed crystals. The calculation is performed by taking S-values of three types of phonon mode and their multiple phonons which were obtained from the analyses of vibronic structures. A guideline, which is always monitored in the simulation studies, is the two points that are characteristics common to the observed band shapes. The first is that the lower-energy slope in the band is about four times the half-width. The second is that the separation between the peak position of the band and the zero-phonon line is nearly equal to one half of the half-width of the band. The latter point just indicates the degree of electron–phonon coupling strength (Fitchen 1968). The simulations of band shapes at around $x = 0$ are composed of three fundamental phonon modes $S = 1.8$, 2.7 and 3.9. With increasing x, multiphonon excitations are incorporated in turn from lower-frequency modes. For $Ca_{0.98}Sr_{0.02}F_2$:Eu, the experimental result at 4.2 K and the computed curve are shown in figure 7, where the three phonon modes T_{1u}, TO_1 and LO_1, and up to their fifth harmonics are considered. The agreement is good except for a slight deviation in the tail of the band shape. We note that, for more precise agreement, neither the

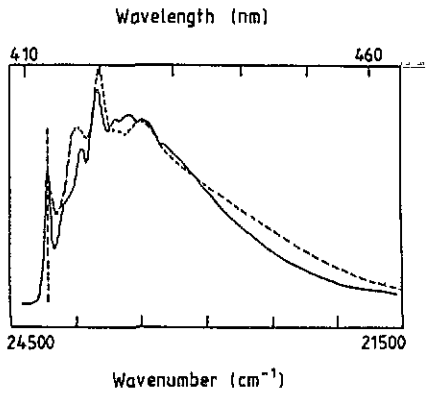

Figure 7. Comparison at 4.2 K for the vibronic structures at $Ca_{0.98}Sr_{0.02}F_2:Eu^{2+}$ of the experimental (——) with the calculated (– – –) results.

induction of other phonon modes nor an increase in the *S*-value of each mode was needed.

5. Conclusions

The luminescence and its vibronic structure were investigated for mixed CaF_2–SrF_2 crystals doped with Eu^{2+} ($4f^7$ ground-state and $4f^65d$ excited-state configurations) ions. The following new results were obtained.

(1) Various optical parameters of the luminescence, i.e. the peak energy, half-width, lifetime and non-radiative activation energy, vary with increasing x, not linearly but quadratically.

(2) The light quenching temperature decreased linearly with increasing x in spite of the non-linear behaviours of the luminescence properties mentioned above.

(3) The temperature dependence of the quantum efficiency and the lifetime revealed that the emission process in this system is a single process emitted from only the lowest Γ_8 level in the excited e_g band.

(4) The analyses of the observed vibronic structures clarified the assistance of several phonon modes in the emission process and suggested an increase in electron–phonon coupling for intermediate x in the mixed crystals although it was still not determinable from estimates of the Huang–Rhys factor.

Acknowledgments

The authors wish to thank Messrs K Miyake, T Ohya, T Yamada and Y Kojima for their partial collaboration in this work. They are also grateful to N Yamada, President of Japan Optical Crystals for the supply of powder materials and appropriate advice on crystal growth. The numerical analyses in this work were performed on the HITAC-M260K computer at the Information Processing Center, The University of Electro-Communications, Tokyo.

References

Baldini G and Guzzi M 1968 *Phys. Status Solidi* **30** 601

Bartolo B D 1968 *Optical Interaction in Solids* (New York: Wiley) pp 378–403
Chase L L 1970 *Phys. Rev.* B **2** 2308
Downer M C, Cordero-Montalvo C D and Grosswhite H 1983 *Phys. Rev.* B **28** 4931
Ehrlich D J, Moulton P F and Osgood R M Jr 1978 *Opt. Lett.* **3** 184
—— 1980 *Opt. Lett.* **5** 339
Fitchen B 1968 *Physics of Color Centers* ed W B Fowler (London: Academic) pp 293–350
Gribier D, Farnoux B and Jacroti J 1962 *Phys. Lett.* **1** 187
Hobden M V 1965 *Phys. Lett.* **15** 10
Kaiser W, Spitzer W G, Kaiser R H and Howarth L E 1962 *Phys. Rev.* **127** 1950
Kawano K, Tominaga J, Satoh H, Nakata R and Sumita M 1990 *Japan. J. Appl. Phys.* **29** L319
McClure D S 1966 *Phonons* ed R W H Stevenson (London: Oliver & Boyd) pp 314–76
McCumber D E 1964 *Phys. Rev.* **134** 299
Rebane K K 1970 *Impurity Spectra of Solids* (New York: Plenum) pp 35–98
Ryan F M, Lehmann W, Feldman D W and Murphy J 1974 *J. Electrochem. Soc.* **121** 1475
Walling J C 1987 *Tunable Lasers* ed L F Mollenauer and J C White (Berlin: Springer) pp 331–98
Weakliem H A 1972 *Phys. Rev.* B **6** 2743